Biosensors and Bioelectronics 146 (2019) 111761

Contents lists available at ScienceDirect

Biosensors and Bioelectronics

journal homepage: http://www.elsevier.com/locate/bios

Dual biorecognition by combining molecularly-imprinted polymer and antibody in SERS detection. Application to carcinoembryonic antigen

Mariana C.C.G. Carneiro [a,b], Ana Sousa-Castillo [c,d], Miguel A. Correa-Duarte [c,d], M. Goreti F. Sales [a,b,*]

[a] BioMark/ISEP, School of Engineering, Polytechnic Institute of Porto, Portugal
[b] CEB, Centre of Biological Engineering, Minho University, Braga, Portugal
[c] Department of Physical Chemistry, Center for Biomedical Research (CINBIO), Universidade de Vigo, Vigo, Spain
[d] Southern Galicia Institute of Health Research (IISGS) and Biomedical Research Networking Center for Mental Health (CIBERSAM), Spain

ARTICLE INFO

Keywords:
Biosensor
Surface-enhanced Raman spectroscopy
Molecularly-imprinted polymer
Carcinoembryonic antigen
CEA-Antibody
Gold nanostars

ABSTRACT

This work reports the innovative combination of a molecularly-imprinted polymer (MIP) and a natural antibody for the accurate surface-enhanced Raman spectroscopy (SERS) detection of carcinoembryonic antigen (CEA). The MIP material acted as a pre-concentration scheme for the target protein, while the natural antibody was responsible to signal the presence of CEA on the MIP platform.

Gold-based screen-printed electrodes were used as substrate and gallic acid (GA) was used herein for the first time in the assembly of a MIP film, by electropolymerization, in the presence of CEA. This layer was further covered by a second ultra-thin film of electropolymerized benzoic acid (BA), to avoid non-specific binding. The rebinding features of the MIP film were evaluated by electrochemical impedance spectroscopy (EIS) and a linear response was observed from 1 to 1000 ng/mL.

For a sensitive SERS detection, the MIP film was first incubated in sample containing CEA and next incubated in SERS tag. For the SERS tag, gold nanostars (AuNSs) were employed as metal support, coupled to 4-aminothiophenol (4-ATP) as Raman reporter and to a natural antibody for CEA as recognition element. The overall system showed a sensitive response down to 1.0 ng/mL, which was different from the blank signal.

Overall, the innovative approach presented herein combines the advantages of using two different targeting elements for CEA. The costs and time of MIP production were substantially low due to selection of electropolymerization approach and the proposal described herein may be extended to other target molecules.

1. Introduction

The earlier diagnosis of cancer is crucial to increase the success rates in cancer treatment (Jayanthi et al., 2017), requiring the intensive involvement of clinicians and wide screening programs. In this regard, the detection of biomarkers in liquid biopsies is emerging as a promising tool (Song et al., 2017). The methods employed for this purpose include polymerase chain reaction (PCR), enzyme-linked immunosorbent assay (ELISA), radioimmunoassay (RIA) or fluorescence immunoassay (FIA), which miss the required portability features to operate in point-of-care (POC), thereby limiting the implementation of large screening schemes aiming at an early detection (Song et al., 2016). Thus, researchers are looking for novel approaches with POC feasibility.

In recent years, the possibility of providing single molecule detection capability, coupled to recent developments that ensured portability features, have made Surface-enhanced Raman scattering (SERS) a serious candidate to be employed in POC (Song et al., 2014; Lu et al., 2015; Ye et al., 2012; Hong and Li, 2013; Joseph et al., 2018; Zhang et al., 2017). Moreover, SERS produces high sensitive data, with fingerprint information, with very little amounts of sample and with multiplex feasibility (Jayanthi et al., 2017; Wang et al., 2016; Lin et al., 2016). In general, SERS provides an enhancement of the Raman features from adsorbed molecules on noble metal surfaces that occurs due to electromagnetic and chemical effects. The presence of localized high electromagnetic fields in the junctions of the metal nanoparticles (NPs) commonly defined as hot-spots is the major responsible for the signal enhancement (Ye et al., 2012; Hong and Li, 2013; Gabudean et al., 2011).

* Corresponding author. School of Engineering of the Polytechnique School of Porto, R. Dr. António Bernardino de Almeida, 431, 4249-072, Porto, Portugal.
E-mail addresses: mgf@isep.ipp.pt, goreti.sales@gmail.com (M.G.F. Sales).

https://doi.org/10.1016/j.bios.2019.111761
Received 9 August 2019; Received in revised form 1 October 2019; Accepted 3 October 2019
Available online 8 October 2019

However, the excellent recognition capabilities of SERS are not sufficient to detect cancer biomarkers in complex samples, such as liquid biopsies, due to the multiple interferences that occur in this medium. To this end, a biorecognition element may be coupled into the metal surface, capturing the target biomolecule and separating it from other components of the sample. Antibodies are the most common elements employed for this purpose (Jayanthi et al., 2017; Wang et al., 2016; Chon et al., 2009). Usually, a sandwich immunoassay procedure is employed, using the metal NP coated with antibody and a Raman reporter (SERS tag) and SERS substrates modified with specific antibodies for the target (Song et al., 2014; Zhang et al., 2017; Lin et al., 2016). The amount of antigen is determined indirectly, by measuring the SERS intensity of the Raman reporter. The use of magnetic NPs in this context has also been addressed, leading to an increased sensitivity due to the concentration of the SERS substrates in the laser spot by means of an external magnetic field (Agoston et al., 2016). Similar approaches have been developed using aptamers as biorecognition elements, for a wide range of different targets (Zhang et al., 2017; Li et al., 2017c), from small molecules (Li et al., 2017c; Pang et al., 2016), to proteins (Yang et al., 2017; Feng et al., 2015; Sivanesan et al., 2015) or living organisms (Wu et al., 2016; Sun et al., 2015).

Molecularly-imprinted polymers (MIPs) have also been coupled to SERS for detection purposes (Zhang et al., 2017; Wang et al., 2017). MIP technology enables the production of artificial receptors that mimic the behaviour of natural antibodies. Their main advantages are high selectivity, low cost and possibility of tailoring on demand (Frasco et al., 2017; Vasapollo et al., 2011). Several SERS approaches explored the well-known extraction/purification capabilities of the MIP materials, to target small molecules (Shahar et al., 2017; Feng et al., 2013, 2017; Ji et al., 2017; Hu and Lu, 2016; Gao et al., 2014; Liu et al., 2011; Li et al., 2017a; Xue et al., 2013) or proteins (Lv et al., 2016; Chen et al., 2018). Protein detection has also been achieved by using a MIP surface to capture the glycoprotein and metal NPs containing the SERS reporter and boronate moieties to bind to the glycosylated fraction of the protein (Ye et al., 2014).

Overall, the previous approaches have a strong possibility of playing a major role in future commercial POC devices for protein detection, due to their high sensitivity and detection capabilities, but problems related to non-specific response outcoming from the biorecognition element represent the main limitation of these sensing strategies that need to be solved. Moreover, the biorecognition element should be robust and selective, ensuring that the retrieved signal is accurate.

Thus, this work reports an innovative approach that combines two different biorecognition elements operating sequentially, thereby reducing the non-specific response. Such hybrid sandwich-like assay is composed of a MIP film used to pre-concentrate the sample in a solid substrate, and natural antibodies bounded to the metal NPs containing the Raman reporter as a transducer element.

The selection of a suitable metal support was also considered herein. In this regard, gold nanoparticles (AuNPs) offer unique properties at structural, electronic, optical, and catalytic level, in addition to their biocompability and low toxicity, stability and easy functionalization (Hong and Li, 2013; Wang et al., 2016; Gabudean et al., 2011; Negrín-Montecelo et al., 2018; Sousa-Castillo et al., 2016). Moreover, the production of AuNPs is easily tuned with different sizes and shapes, which hold a great impact upon the signal enhancement. In this regard, there are different morphologies reported, from which Au nanostars (AuNSs) are highly attractive in photocatalysis (Sousa-Castillo et al., 2016) and sensing (Sousa-Castillo et al., 2017). These nanostructures have multiple sharp branches, creating a "lightning rod" effect that enhances intensely the local electromagnetic field, thereby leading to higher magnification of the SERS signals (Vo-Dinh et al., 2018; Wang et al., 2013). Also, the high surface area enables the attachment of more Raman reporter molecules (Wang et al., 2013). Thus, AuNSs were employed herein as signal enhancer.

Regarding the MIP production, the conventional procedure includes combining template and functional/cross-linking monomers in a suitable porogenic solvent. The 3-D polymer network is formed after the addition of an external radical species (of thermal, chemical or electrical origin) and the MIP is obtained after template extraction. Having a protein as template, several restrictions apply to avoid protein denaturation (Frasco et al, 2017; Vasapollo et al., 2011; Erdőssy et al., 2016), involving the use of aqueous solvents with suitable pH and ionic strength.

The kind of radical polymerization conducted is also a critical issue when producing a MIP for a protein. In general, the overall procedure involved in polymerizations initiated by chemical/thermal radicals may take more than one day, while the electrically initiated polymerization (or electropolymerization) may take only few seconds (Wallace et al., 1999). In this, the oxidation of a monomer to a cation radical is followed by the attack on another molecule of the monomer, typically leading to the formation of a radical species; subsequent formations of monomeric or dimeric radicals lengthen the polymeric chain, and repeated formations produce the final polymer (Vidal et al., 2003). Because it is carried out under mild conditions, the entrapment of biological molecules is allowed without affecting their biological/biochemical activity (Vidal et al., 2003). Moreover, the electrochemical polymerization is simple and reproducible; forming polymeric films with thicknesses that range from 5 to 1 μm, being easily adjusted by controlling the electrochemical conditions employed (Frasco et al., 2017; Erdőssy et al., 2016; Vidal et al., 2003; Zoski, 2007). Additionally, the costs related to electropolymerization are also much lower.

To implement an electropolymerization procedure, a 3-electrodes cell is required. To this end, there are several commercial screen-printed electrodes (SPEs) that may be employed for this purpose, which just need less than 70 μL of the polymerizing solution, thereby contributing to additional cost decrease. This is particularly relevant when proteins are used as targets, because the reagents involved are very expensive.

Finally, the target protein selected in this work was carcinoembryonic antigen (CEA). CEA is a glycoprotein (≈180 kDa) overexpressed in several malignant tumours as pancreatic carcinoma, colorectal cancer, gastric cancer, lung cancer and breast carcinoma (Song et al., 2017; Wang et al., 2016). The main SERS assays reported for CEA detection have been resumed in Table 1.

From these, it is clear that the use of AuNSs and Au-coated magnetic nanomaterials allowed reaching very low detection limits. However, it is important that the linear response range observed must be tuned with the CEA existing in the circulating fluids. In this regard, CEA serum concentrations in healthy people are usually under 10 ng/mL, while in people with malignant tumours, this level is higher than 20 ng/mL (Song et al., 2017).

Thus, this work describes a SERS sandwich-like approach combining MIP and antibody as biorecognition elements for providing sensitive and accurate signals. The MIP was assembled by electropolymerizing GA on the gold working electrode of a commercial SPE and the antibody was bound to the AuNSs loaded with 4-aminothiophenol (4-ATP) as the Raman reporter molecule (AuNS@4ATP@Ab). The operational procedure consisted in incubating first the sample in the MIP film for a given time, washing the surface with buffer and incubating there AuNS@4ATP@Ab, for subsequent Raman reading. The critical variables were optimized and the system was tested in spiked samples.

2. Experimental

2.1. Reagents and solutions

All chemicals were of analytical grade and water was ultrapure Milli-Q laboratory grade. Potassium hexacyanoferrate II-3-hydrate ($K_4Fe(CN)_6 \cdot 3H_2O$), potassium hexacyanoferrate III ($K_3Fe(CN)_6$), sodium phosphate dibasic dihydrate ($Na_2HPO_4 \cdot 2H_2O$) and sodium dihydrogen phosphate dihidrate ($NaH_2PO_4.2H_2O$) were purchased from Riedel de

Table 1
Previous works based on a sandwich SERS assay using labelled NPs modified with CEA antibody as probe for CEA detection.

Methodology		Response range (ng/mL)	LOD (ng/mL)	Reference
SERS Substrate	SERS Probe			
Au butterfly wings	CEA aptamer@RohdG	10 to 10000	10	Song et al. (2017)
AuMNPs	AuNF@4-MBA	0.01–100	0.00148	Song et al. (2016)
AuMNPs	AuNF@4-MBA	0.00000001 to 1	0.00000001	Song et al. (2014)
Electrode modified, chitosan stabilized AuNPs	AuNP coated resin microsphere@NBA	1800 to 18000000	0.01	(Lu et al., 2015)
AuNS	AuNS@4-MBA	0.01 to 1000	—	Wang et al. (2016)
AuNP@Fe_2O_3	AuNP@4-MBA	1 to 50	0.1	Lin et al. (2016)
Ordered gold nanohoneycomb arrays	AuNS@4-MBA	0.5 to 100	0.44	Li et al. (2017b)
magnetic beads	HGN@MGITC	0 to 20	1.67	Chon et al. (2011)
Au-SPEs modified with a MIP	**AuNS@4ATP**	**1 to 1000**	**1**	**This work**

AuMNPs: gold-coated magnetic nanoparticles; AuNFs: gold nanoflowers; AuNPs: gold nanoparticles; AuNSs: gold nanostars; Au-SPEs: gold screen-printed electrodes; CEA: Carcinoembryonic antigen; DMSA: dimercaptosuccinic acid; Fe_2O_3: ferric oxide; HGNs: hollow gold nanospheres; MBA: 4-mercaptobenzoic acid; MIP: molecularly-imprinted polymer; MGITC: malachite green isothiocyanate; NBA: Nile Blue A; RohdG: Rohdamine Green; SERS: surface-enhanced Raman scattering.

Haën; *N,N*-Dimethylformamide (DMF) (C_3H_7NO) and tri-sodium citrate dihydrate ($C_6H_5Na_3O_7 \cdot 2H_2O$) were purchased from Analar Normapur; ethanol absolute (C_2H_5OH) ≥99.9%, tetrachloroauric acid ($HAuCl_4 \cdot 3H_2O$), polyvinylpyrrolidone (PVP, $(C_6H_9NO)_n$) with molecular weight 10.000, BA ($C_7H_6O_2$), thionine acetate salt ($C_{12}H_9N_3S \cdot C_2H_4O_2$), toluidine blue ($C_{16}H_{16}IN_3S$), 4-mercaptobenzoic acid (4-MBA, $C_7H_6O_2S$) 99% and monoclonal anti-CEA antibody produced in mouse were purchased from Sigma Aldrich; cysteamine hydrochloride ($C_2H_7NS \cdot HCl$) was purchased from Merck; 4-ATP (C_6H_7NS) 96% was purchased from Acros Organics; GA ($C_7H_6O_5 \cdot H_2O$) monohydrate ≥99% HPLC, hydrochloric acid (HCl) 37% and nitric acid (HNO_3) 70% were purchased from Panreac; CEA antigen from human fluids was purchased from EastCoast Bio.

Stock solutions of CEA antigen and CEA antibody were prepared in phosphate buffer (0.0729 M Na_2HPO_4 and 0.0171 M NaH_2PO_4, pH = 7.4).

All glassware and magnetic stir bars used in the synthesis of AuNPs were cleaned in aqua regia (HCl/HNO_3, 3:1) and rinsed in ultrapure water to prevent unwanted nucleation and aggregation of gold colloid solution during the synthesis.

2.2. Apparatus

The electrochemical measurements were conducted at PGSTAT302N, a potentiostat/galvanostat from Metrohm Autolab equipped with a FRA module and controlled by Nova 2.1 software. The Au-SPEs (DRP-C220AT, DropSens) contained a gold working electrode (4 mm), a gold counter electrode and a reference electrode, having electrical contacts made of silver. A switch box, also from *BioTID Electrónica*, was interfaced between the SPEs and the equipment.

Raman studies were performed on a DXR Raman Spectrometer, from Thermo Fisher Scientific Company, using the Thermo Scientific OMNIC Software. The spectra were acquired in the range from 300 to 1800 under, using a 785 nm excitation laser, through a 50 × confocal microscope objective. The laser power was adjusted to 5 mW, with an aperture of 50 μm slit, for 10 s acquisition time. In addition to this equipment, the inVia™ confocal Raman microscope from Renishaw was used. In this case, the range from 100 to 3500 was selected, also using a 785 nm excitation laser, and a 50 × confocal microscope objective. The laser power was 0.16 mW for 10 s acquisition time.

UV–Vis studies were made in the UV–Visible Spectrophotometer Evolution 220, from Thermo Fisher Scientific Company. Transmission electron microscopy (TEM) was performed using a JEOL JEM 1010 transmission electron microscope operating at an acceleration voltage of 100 kV.

2.3. Electrochemical assays

Electrochemical assays were performed in equimolar amounts of the standard redox probe potassium ferrocyanide and potassium ferricyanide (5.0×10^{-3} M), prepared in phosphate buffer (0.0729 M Na_2HPO_4 and 0.0171 M NaH_2PO_4), pH 7.4. All measurements were made at room temperature. Between measurements and incubations, the electrodes were rinsed in ultrapure water and softly dried under flowing nitrogen gas.

Electrochemical impedance spectroscopy (EIS) assays were made under 0.2 V, with a sinusoidal potential perturbation of 0.01 V amplitude and 10 frequencies per decade, over 0.1 to 1×10^5 Hz frequency range. Square wave voltammetry (SWV) measurements were made in a potential window from -0.2 to +0.5 V, at a frequency of 1 Hz, and a step height (amplitude) of 0.02 mV.

Electropolymerization of suitable monomers made by cyclic voltammetry (CV). GA was electropolymerized between -0.2 and 0.8 V, at a scan rate of 0.025 V/s for 10 cycles, with a pre-accumulation of 20 s at 0.22 V. BA was electropolymerized between 0 and 0.9 V, at a scan rate of 0.025 V/s for 1 cycle.

2.4. Fabrication of the MIP film

The MIP film was assembled on the working electrode area of the Au-SPEs, according to the schematic representation shown in Fig. 1. First, the Au-SPEs (Fig. 1A) were rinsed with absolute ethanol to remove impurities, and modified by a self-assembled monolayer with cysteamine (5.0×10^{-2} M) for 1 h (Fig. 1B). A solution containing the monomer (GA, 1.0×10^{-4} M) and the target template (CEA, 200 μg/mL) prepared in buffer was then placed on top of the 3-electrodes and underwent the electropolymerization procedure (Fig. 1C). Unreacted monomer species or small oligomers were removed by washing and consecutive CV cycles in phosphate buffer, until a stable electrochemical signal was reached. After this, a single CV cycle of BA solution was made to stabilize the final film and avoid nonspecific adsorption. The template was removed by incubating 2.5 μL of an ethanol aqueous solution (ethanol/water, 3:7) in the working electrode, for 1 h (Fig. 1D).

Non-imprinted polymers (NIPs) acting as control were also produced, by means of the same protocol without adding CEA protein at the electropolymerization solution.

2.5. Production of the AuNSs

The AuNSs were synthesized through a seed-mediated growth method, requiring the AuNPs previously prepared that were obtained by the classical method described by Turkevich (Turkevich et al., 1951), through the reduction of tetrachloroauric acid by tri-sodium citrate. The AuNPs were prepared from a tetrachloroauric acid (50 mL, 5.0×10^{-4} M) solution that was boiled under vigorous stirring and added of tri-sodium citrate (5 mL, 3.4×10^{-2} M) solution. This mixture changed the colour of the final solution from pale yellow to transparent, black and finally dark red (signalling the formation of AuNPs). The

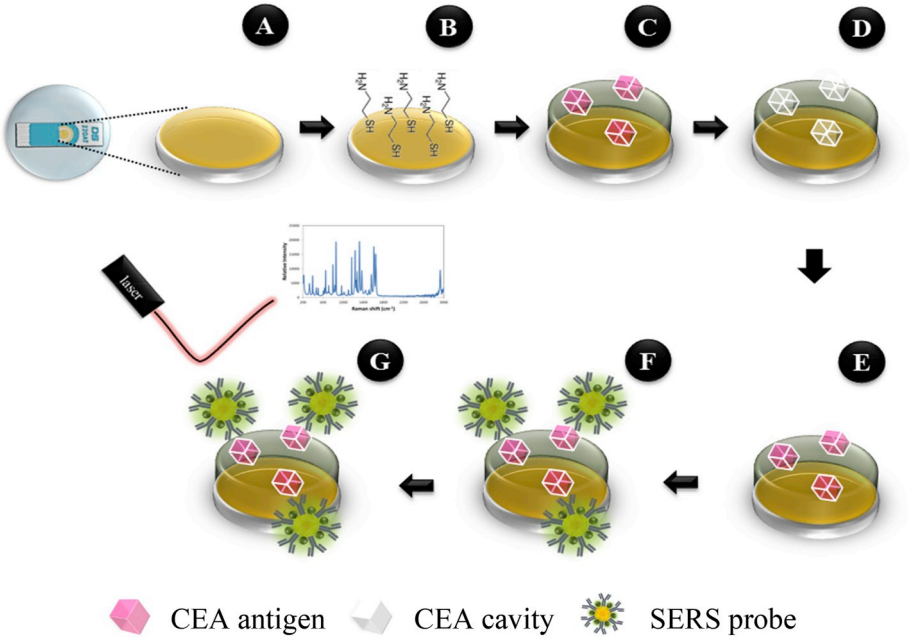

Fig. 1. Schematic representation of the assembly of the biosensor. Cleaning step (A), surface modification (B), electropolymerization (C), removal step (D), rebinding (E), bound of the SERS probes (F) and signal measurement (G).

resulting solution was kept for 20 min at boiling temperature (Turkevich et al., 1951). The synthesized AuNPs were characterized using UV–vis spectrophotometry.

After this, the surface of the AuNPs was covered by slowly adding a PVP solution (5 mL, 3.0×10^{-2} g/mL) and maintaining it under stirring for 24 h. Then, the solution was submitted to sequential centrifugation steps to remove the supernatant water and re-suspend the particles in ethanol. The absorbance was measured at this point to check the concentration. In parallel, a solution of PVP was prepared in DMF (100 g/L) and quickly added to a tetrachloroauric acid solution (0.1056 M), keeping it under stirring for 5 min, in a cold bath. Subsequently, the previous AuNPs solution was added into this one, keeping it under stirring for 45 min, in an ice-bath. During this mixture, the colour of the solution changed from yellow to red and finally dark blue (Pandian et al., 2008). Again, centrifugation steps allowed removing DMF, and the resulting solid was re-suspended in ethanol. The absorbance of the formed AuNSs was measured and the stock solution was stored at 4 °C for further use.

2.6. Fabrication of the SERS tag

A SERS tag is generally produced by attaching to the surface of metal NPs (one or more, for multiplex analysis) the Raman reporter that provides a known Raman spectrum and a biorecognition element, as an antibody for specific binding to the target. In addition, a protective shell could be added for biostability and biocompability (Song et al., 2014; Wang et al., 2013).

2.6.1. Selection of the Raman reporter

Four possible Raman reporters were tested herein: 4-ATP, 4-MBA, thionine acetate salt and toluidine blue. Tests were made with 200 µL of each reporter molecule (1.0×10^{-5} M, in ethanol) added of 200 µL of the AuNSs (0.6 mM), previously prepared and stirring for 1 h. After a centrifugation step (4500 rpm, for 45 min) to remove the supernatant, 100 µL of phosphate buffer were added to re-suspend the particles.

The Raman response of these tags was evaluated by casting the solution of the working electrode area of the commercial Au-SPEs used in the MIP film assembled. For this purpose, the Au-SPEs were cleaned with ethanol, modified with cysteamine (5.0×10^{-2} M) for 1 h, and added of 2.5 µL of AuNS@4-MBA, AuNS@4-ATP, AuNS@thionine or AuNS@toluidine. These reporter solutions were kept on the SPEs for 1 h, and the Raman spectra were acquired next.

2.7. CEA-antibody binding

The CEA antibody solution (20 µL, 1.0×10^{-4} g/mL) was added to the solution containing the AuNSs (200 µL, 6.0×10^{-4} M) and the selected Raman reporter, 4-ATP (200 µL, 1.0×10^{-5} M), and kept under stirring for 7 h. After a centrifugation step, phosphate buffer (200 µL) was added and the SERS probes (AuNS@4ATP@CEA antibody) were ready to use.

2.8. SERS procedure for CEA detection

The detection of CEA started by incubating in the MIP film a blank solution and CEA standard solutions of increasing concentrations (1 and 1000 ng/mL), on the working electrode area (where the MIP film was assembled), for a period of 30 min (Fig. 1E). After this, the surface was washed and 2.5 µL of SERS probes (AuNS@4ATP@Ab) were incubated overnight (Fig. 1F) in the same spot. The Raman spectra were acquired next (Fig. 1G).

3. Results and discussion

3.1. Construction of the MIP

The MIP film was assembled by electropolymerization, using a cyclic potential scan in CV (Wallace et al., 1999). Herein, the rate of film deposition was defined by the scan-rate of potential change in each cycle and the number of consecutive cycles established in the overall procedure. GA was selected for this purpose. It contains an aromatic ring with several hydroxyl groups that allow the formation of hydrogen bridges with the target template. Moreover, it requires a low potential for its oxidation, and subsequently its electropolymerization, supported by the fact that it acts as an antioxidant. This is the first time this compound is used as single monomer to assemble a MIP film. Prior to electropolymerization, the gold working electrode was cleaned and modified with a thiol compound to ensure that the polymer layer would

be suitably attached to it. Fig. S1 shows the consecutive CVs made for the electropolymerization of GA in the presence of CEA. The first scan of the voltammogram showed the typical oxidation peak of GA with an anodic peak potential (Ep_a) around 0.63 V. The current intensity of the anodic peak (Ip_a) value decreased over the several cycles, thereby confirming the deposition of a polymer on the working electrode area and that this polymer corresponded to an insulating film.

All chemical modifications occurring at the electrode surface were followed by electrochemical techniques, using a standard iron redox probe that keeps the same concentration and ionic strength throughout the experiments. As each step is implicated in a different chemistry, any change in the electrical properties detected by reading this redox probe is signaling the inherent chemical changes occurring in each step of the assembly process. SWV was used for this purpose, monitoring the peak current intensity (Ip_a), as well as EIS, monitoring the charge transfer resistance (*Rct*) of the Randles equivalent circuit including the Warburg element (W) for diffusion. Fig. 2 shows the electrochemical signals recorded along the several stages of the biosensor construction. The formation of a polymeric film was confirmed by a significant reduction of the Ip_a in SWV and a consistent increase of the *Rct* in EIS. This behaviour was more intense in the MIP film, due to the presence of the CEA within the polymeric network, a non-conductive element. In the next stage of modification, the same behaviour was observed after the stabilization performed by CVs in phosphate buffer and after the polymerization of BA; this reflected the removal of unreacted molecules or small oligomers standing on the surface. This behaviour changed after the removal step of CEA in the MIP film, yielding an increase in the peak current of SWV and a decrease of *Rct* in EIS. This removal step did not promote significant changes in NIP surface, because there was no CEA to be removed from it. Overall, the final peak current of the MIP was lower than that of the NIP, and the R_{ct} was higher. This was most likely related to the partial entrapment of CEA molecules inside the polymeric network, even after the template removal stage.

Some optimization experiments were performed, namely regarding the concentration of imprinted CEA. Electropolymerization was performed according to the conditions previously described, for 100 μg/mL and 200 μg/mL. Relative R_{ct} plots are presented in Fig. S2. The MIP film imprinted with 200 μg/mL displays an increase in R_{ct} value that corresponds of 115% to the MIP film imprinted with 100 μg/mL, which indicates more charge transfer resistance. These results could be due to the presence of a high amount of protein, thus increasing the number of formed cavities that will enable the rebinding of more template molecules, increasing the sensitivity of the biosensing film. Thus, a concentration of 200 μg/mL of CEA was selected for the imprinting step in further experiments.

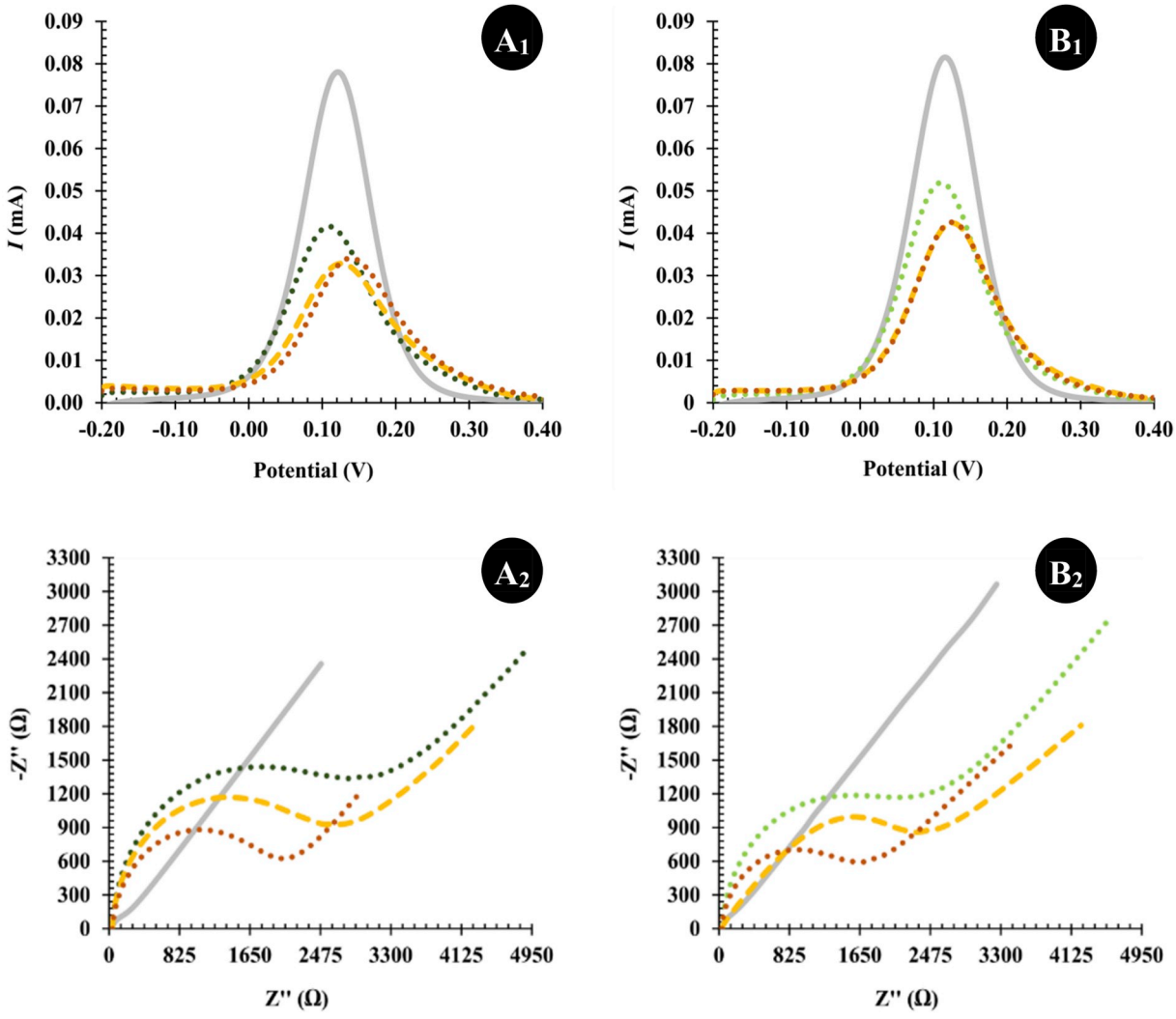

Fig. 2. SWV (1) and EIS (2) measurements of the different steps of the MIP (A) and NIP (B) construction: cleaning (——); polymerization of MIP/NIP films (● ● ●/● ● ●); stabilization and BA film (— — —); and template removal (● ● ●).

3.2. CEA rebinding from the MIP film

The stability of the sensing film before CEA rebinding was essential to ensure that the signal output was correct. To this end, the surface was stabilized by successive incubations in phosphate buffer, for 30 min. The EIS readings were made after each incubation period, until the R_{ct} value was consistent with the previous measurement. Fig. S3 shows different electrodes prepared at the same time may, needing from 1 to 4 buffer incubation steps until the a stable signal was reached, and leading to similar R_{ct} values before the calibration.

The rebinding features of the biosensor were assessed by calibrating the MIP film with CEA standard solutions ranging from 0.1 to 1000 ng/mL. To this end, the biosensing film was incubated in each standard solution for 30 min; after this, this solution was washed out and replaced by the iron redox probe to carry out EIS evaluations. The data so obtained is shown in Fig. 3, with calibrations plotting R_{ct} in EIS against log CEA concentration shown in Fig. S4.

In general, the rebinding of CEA to the complementary MIP cavities contributed to an increase in the charge transfer resistance by the iron redox probe, and thus an increase in the R_{ct} value with the increasing CEA concentration. The linear response of R_{ct} in EIS changes against the logarithm CEA concentration was observed from 1.0 ng/mL until 1000 ng/mL, in the MIP film, corresponding to R_{ct} (Ω, open circuit potential) = 92 × log(CEA, ng/mL) + 1667 (R-squared 0.9958). The detection limit, calculated considering the slope of the linear portion of the calibration curve was <0.5 ng/mL. Thus, the linear response observed and the CEA response concentration range of the biosensing film covered the concentration range of clinical interest.

In contrast, the observed R_{ct} values of the NIP film kept almost the same with the increasing of CEA concentration. This behaviour is probably reflecting the absence of the complementary cavities formed by molecular imprinting and the existence of an outer surface made of only poly(BA). Since there was no template to be removed from it, the final layer was only poly(BA) and the proteins interacting with this surface had probably no access to the poly(GA) layer, where the proteins were imprinted on the MIP.

3.3. Reduction of non-specific response

To avoid adsorption of non-specific species, a layer of BA was added after the MIP construction, by electropolymerization. Fig. S6 shows calibration plots of MIP films with and without BA layer. It could be observed that the response of the sensor without BA layer is random when compared with the linear response of the sensor with BA layer. In general, it is expected that the presence of –COOH groups from the BA shall decrease the non-specific protein binding to the sensing surface.

3.4. Selectivity assay

Selectivity studies were made by incubating on the MIP film a mixed solution of target protein and an interfering compound, prepared in the background buffer. CA15-3, a cancer biomarker protein was selected as interfering species. A solution containing CEA (10 ng/mL) and CA15-3 (30 ng/mL) was incubated on the working electrode for 30 min. EIS measurements were carried out to evaluate the selectivity of the sensor, comparing with an electrode were only CEA (10 ng/mL) was incubated.

According to Fig. 4, it can be observed that the binding of CEA (Fig. 4A) showed a R_{ct} increasing of 13.1% to the signal of buffer stabilization, while the binding of a solution containing CEA and CA15-3 displayed a negligible signal variation.

3.5. Preparation and characterization of the AuNSs

The adopted procedure combines the reduction power of DMF and uses PVP as a stabilizer, as well as sonication as energy source to produce AuNSs, from the preformed AuNPs seeds, with a high number of sharp tips which is expected to increase SERS activity (Kumar et al., 2008). In this procedure, an acid solution of tetrachloroauric acid is the precursor, being reduced by a basic solution of sodium citrate (Agunloye et al., 2017; Shi et al., 2017). Citrate also acts as a pH mediator and has a role as stabilizing agent, preventing the aggregation and precipitation and leading to stable monodispersed AuNPs with a controlled size distribution (Wang et al., 2013; Agunloye et al., 2017; Shi et al., 2017). PVP has been used not only as a stabilizer agent in the synthesis of metal NPs, preventing their aggregation and improving the stability in organic solvents, but also, when used in combination with external energy sources as ultrasounds, it could be a reducing agent. In this procedure, DMF also acts as a reducing agent in PVP molecules, controlling the reduction kinetics of tetrachloroauric acid ions on the preformed AuNPs seeds (Kumar et al., 2008).

The AuNSs obtained herein were characterized by TEM and UV/Vis-NIR spectrophotometry (Fig. 5). TEM images from isolated AuNSs revealed a solid core surrounded by several sharp, irregular and short branches (Fig. 5A and B). Moreover, images collected with several AuNSs suggested that the particles had similar sizes and were individually dispersed and not aggregated (Fig. 5C and D). Also, a distribution analysis (Fig. S7) based on TEM images allow us to calculate the average size of the particles, being the core of AuNSs about 25.6 ± 1.5 nm. Spikes

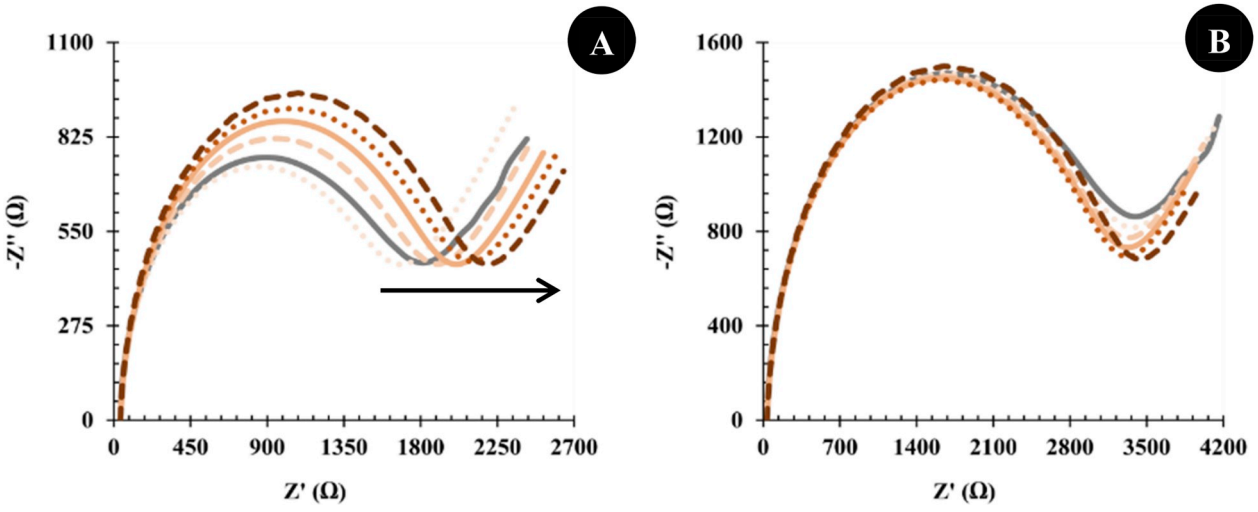

Fig. 3. EIS measurements of buffer stabilization (——) and increasing standard concentrations of CEA 0.1 (• • •), 1 (– – –), 10 (——), 100 (• • •) and 1000 (– – –) ng/mL of the MIP (A) and NIP (B) films.

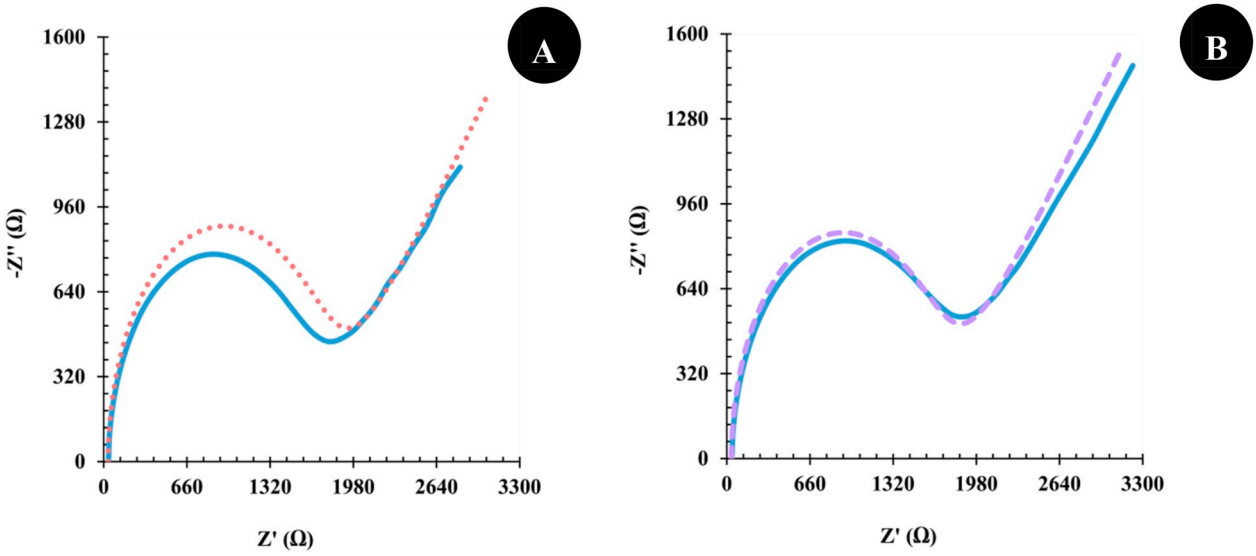

Fig. 4. EIS measurements of buffer stabilization (——), CEA 10 ng/mL (• • •) and CEA 10 ng/mL + CA15-3 30 U/mL (– – –).

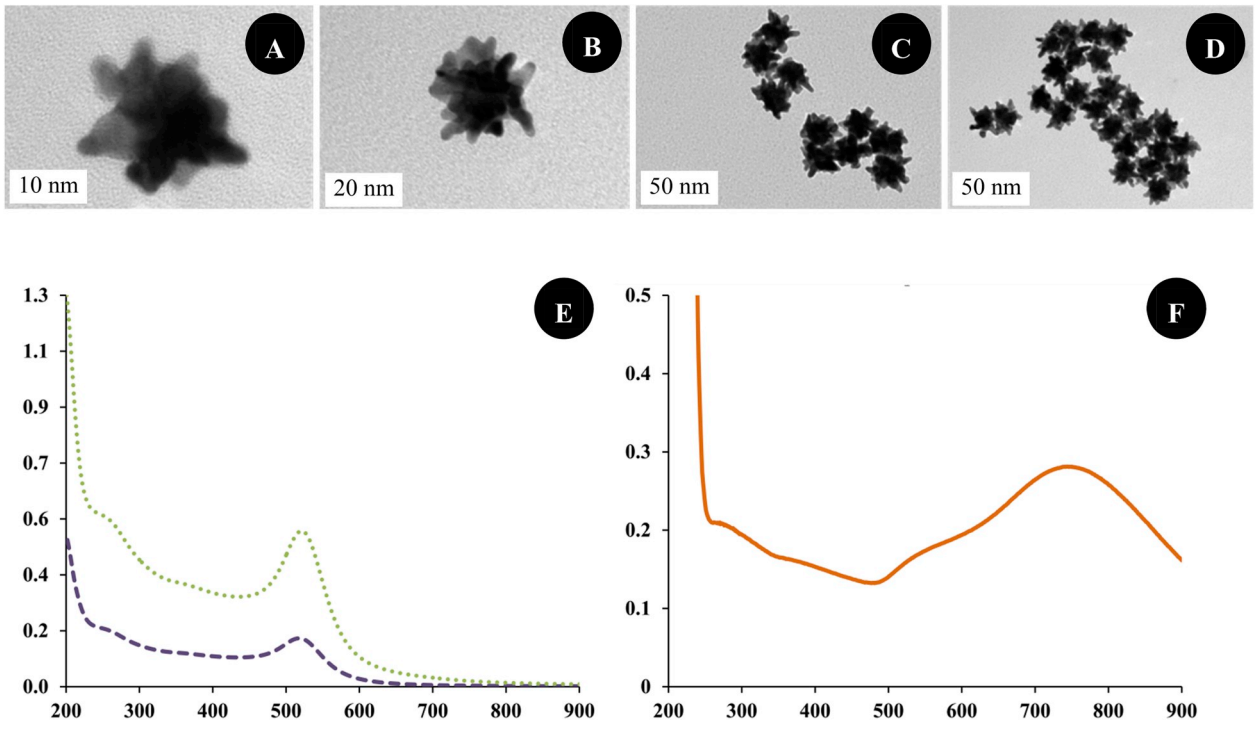

Fig. 5. TEM images of the AuNSs with low (A, B) and high magnification (C, D); UV–vis–NIR spectrum of the produced AuNPs (E) before (– – –) and after (• • •) covering with PVP and AuNSs (F) (——).

length can vary between 6 and 15 nm, by tuning the ($HAuCl_4$):(Au seed) ratio for the preparation of particles.

AuNPs and AuNSs production steps were followed by UV/Vis-NIR and are in agreement with TEM results (Fig. 5E and F). Based on the theoretical knowledge that a value of 1.2 a.u. of absorbance at 400 nm corresponds to a concentration of 0.5 mM (Scarabelli et al., 2015), AuNPs concentration was estimated to be 0.42 mM (corresponding to an absorbance of ~ 0.10 a.u.). The addition of PVP into AuNPs yielded a red shift of maximum absorption peak (from 518 nm to 521 nm) due to a change in the refractive index of the solution caused by a change of the solvent (from water to ethanol). In addition, it can be observed a significant absorbance increase (from 0.16 a.u to 0.51 a.u.) that occurs due to the increasing concentration of the sample during the centrifugation step.

The spectra of AuNSs (Fig. 5F) evidenced significant differences when compared to that of AuNPs alone or with PVP. The peaks became into broad absorbance areas, from which two plasmon bands may be underlined: (i) a smaller broad shoulder absorption is located between 500 and 600 nm, representing the core of the particle; (ii) and a maximum absorption peak of ~ 0.28 a.u. is located after this, until the NIR region of the spectra, with a maximum value around 740–750 nm, representating the outer spikes of AuNSs (Wang et al., 2013). Also, a concentration of 0.64 mM in AuNSs solution was estimated from the absorbance at 400 nm (Scarabelli et al., 2015) (~ 0.15 a.u.).

3.6. Selection of the Raman reporter

The selection of a suitable reporter is critical in SERS because it is the spectra of this compound that shall be enhanced under Raman spectroscopic analysis and so their absorption wavelength should be taken into account. Raman reporter molecules need to be attached onto the surface of the AuNSs and their interaction should be strong. Molecules with functional groups containing nitrogen or sulphur are usually used as Raman reporters, due to their affinity to silver or gold NPs used as SERS substrates. Also, an optimal coverage and a uniform orientation of the reporter onto the surface of the metallic NP should be considered, in order to ensure the maximum SERS sensitivity and reproducible spectra (Wang et al., 2013).

Herein, four different Raman reporter molecules were tested. 4-ATP (Ye et al., 2012), 4-MBA (Song et al., 2016), thionine (Lu et al., 2015) and toluidine (Shashni et al., 2017) have been employed in this context, because these are inexpensive materials, with high affinity to the gold NPs and promptly available (Wang et al., 2013).

The results obtained with the several reporters are shown in Fig. 6A and show a clear different behaviour from 4-ATP. Overall, the reporters were all tested in the same conditions and 4-ATP has a great intensity of signal. The main bands in SERS spectra of 4-ATP were assigned to the a_1 modes at 1079 cm^{-1} and 1587 cm^{-1}, due to the stretching vibrations of C–S and C–C, respectively (Gabudean et al., 2011). The peak at 1079 cm^{-1} was used to follow the Raman response, and suggested in previous works (Hong and Li, 2013). Thus, 4-ATP was the selected for further tests.

3.7. CEA monitoring with SERS

As proof-of-concept of the principle behind this paper, two distinct concentrations of CEA were incubated in the working electrode containing the MIP film. The concentrations selected for this purpose were 1.0 and 1000 ng/mL, very different from each other and within the concentration range of response of the MIP film. Control tests were also made by incubating a blank solution in both MIP and NIP films, and incubating a 1000 ng/mL CEA solution in the NIP film. After this, the SERS tags were incubated on the working electrode area.

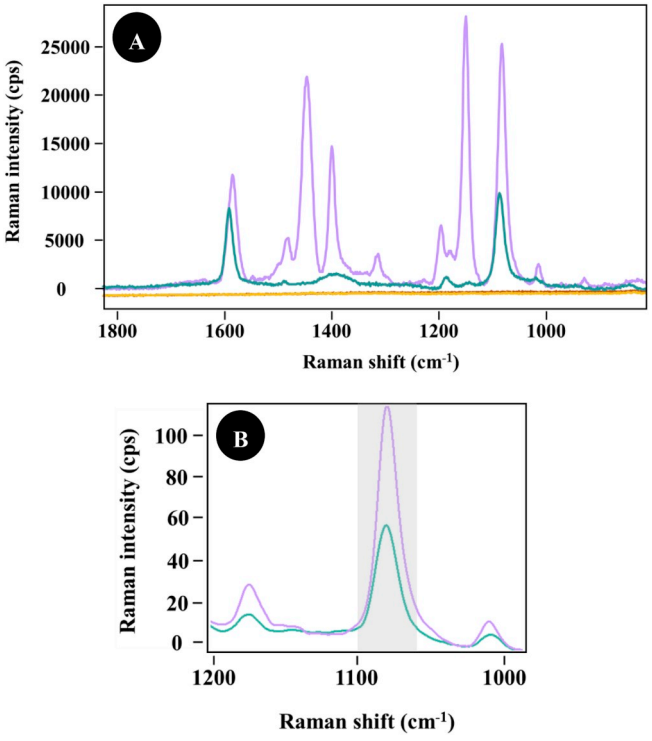

Fig. 6. Raman spectra of (A) AuNS@4-ATP (—), AuNS@4-MBA (—), AuNS@thionine (—) and AuNS@toluidine (—), immobilized onto Au-SPEs modified with cysteamine, and (B) of AuNS@4ATP@CEA antibody in a MIP with 1 ng/mL (—) and 1000 (—) ng/mL of CEA.

The Raman spectra were collected after, randomly, picking different spots in the working electrode area. The peak followed-up for quantitative purposes was located at 1079 cm^{-1} Raman shift, which would monitor indirectly the concentration of CEA. This peak should be detected only when CEA was adsorbed on this surface, meaning that the CEA-antibodies linked to the AuNPs@4ATP would bind to it, and that this signal would be higher for a higher concentration of CEA.

The spectra obtained for the MIP materials are shown in Fig. 6B. Blank NIP and MIP and also NIP with the highest amount of CEA spectra are presented in Fig. S5. The corresponding data is presented in Table S1. In general, the concentration of 1.0 ng/mL was clearly different from the blank signal, increasing in 151% the signal of the blank. The maximum concentration tested (1000 ng/mL) was much higher in terms of Raman signal, corresponding to an increase of 330% to the signal of the blank. Overall, this data revealed that the system was yielding the expected information, with higher concentrations of CEA leading to a higher intensity of the 1079 cm^{-1} Raman shift peak.

As expected, the NIP film incubated in the maximum concentration of CEA showed a weak Raman signal, even when compared to the lowest concentration of CEA incubated in the MIP film (Table S1). This behaviour accounted most particularly the absence of a non-specific binding event on the NIP. In the eventual case of occurring a non-specific CEA binding (which did not happen), the antibody Raman probe would have detected the CEA in this surface, leading to a higher 4-ATP signal. In turn, this also confirms that the rebinding of CEA to the MIP film was dominated by adsorption at the specific rebinding sites existing on this layer. Moreover, the blank control of both MIP and NIP surfaces showed low intensity Raman signals (Table S1), because the Raman probes could not specifically bind to it, due to the absence of CEA.

4. Conclusions

This work describes the successful production of a MIP film for CEA rebinding in a concentration dependent manner. This MIP film was further used to concentrate the target protein and the Raman reporter used to detect it by means of a CEA-antibody linked to it. This innovative combination solves the problems generated by SERS detection in sandwich approach using only MIP materials or natural antibodies. Moreover, the production of the MIP film was made *in-situ*, and the procedure involved in the production of a ready-to-use electrode took less than 3 h, which costs about 4 € in reagents per unit electrode. The clinical usefulness of the device is clear, as the proposed approach is able to detect concentrations within the clinical range of interest for CEA, in which cancer disease is suspected >10 ng/mL.

Overall, the results confirmed the accuracy of the detection of CEA and the possibility of generating quantitative information. In addition to this, the combination of MIP and antibody for SERS detection was considered an excellent alternative to current methods. The MIP film acted as a pre-concentrating system, by increasing the possibility of having the target protein on the surface, while the antibody linked to the Raman reporter ensured that the protein being detected was the one intended. Even if some interfering proteins would adsorb into the MIP film, the possibility of having a significant response from a non-specific response of the natural antibody is quite low, because the ratio of the proteins shall favour the targeted species. The proposed device may be further extended to other cancer biomarkers, with benefits in terms of costs and analytical features.

Declaration of competing interest

The authors declare that they have no known competing financial interests or personal relationships that could have appeared to influence the work reported in this paper.

CRediT authorship contribution statement

Mariana C.C.G. Carneiro: Investigation, Data curation, Methodology, Validation, Writing - original draft. **Ana Sousa-Castillo:** Investigation, Data curation, Methodology, Writing - original draft. **Miguel A. Correa-Duarte:** Conceptualization, Funding acquisition, Data curation, Writing - review & editing. **M. Goreti F. Sales:** Conceptualization, Supervision, Project administration, Writing - original draft.

Acknowledgements

Authors acknowledge funding to FEDER/COMPETE 2020 through the project RamSERS (NORTE-01-0247-FEDER-017834, call no. 33/SI/2015), to POCTEP through the project IBEROS (0245_IBEROS_1_E), Fundação para a Ciência e Tecnologia, I.P., through the PhD grant reference SFRH/BD/131959/2017, MINECO-Spain CTM2017-84050-R and Xunta de Galicia (IN607A 2018/5 and Acc. 2016–2019).

Appendix A. Supplementary data

Supplementary data to this article can be found online at https://doi.org/10.1016/j.bios.2019.111761.

References

Agoston, R., Izake, E.L., Sivanesan, A., Lott, W.B., Sillence, M., Steel, R., 2016. Nanomed. Nanotechnol. 12 (3), 633–641.
Agunloye, E., Gavriilidis, A., Mazzei, L.A., 2017. Chem. Eng. Sci. 173, 275–286.
Chen, S., Dong, L., Yan, M., Dai, Z., Sun, C., Li, X., 2018. Roy. Soc. Open Sci. 5 (1), 171488-171488.
Chon, H., Lee, S., Son, S.W., Oh, C.H., Choo, J., 2009. Anal. Chem. 81 (8), 3029–3034.
Chon, H., Lee, S., Yoon, S.Y., Chang, S.I., Lim, D.W., Choo, J., 2011. Chem. Commun. 47 (46), 12515–12517.
Erdőssy, J., Horváth, V., Yarman, A., Scheller, F.W., Gyurcsányi, R.E., 2016. Trends Anal. Chem. 79 (Suppl. C), 179–190.
Feng, J., Wu, X., Ma, W., Kuang, H., Xu, L., Xu, C., 2015. Chem. Commun. 51 (79), 14761–14763, 2015.
Feng, S., Gao, F., Chen, Z., Grant, E., Kitts, D.D., Wang, S., Lu, X., 2013. J. Agric. Food Chem. 61 (44), 10467–10475.
Feng, S., Hu, Y., Ma, L., Lu, X., 2017. Sens. Actuators B 241, 750–757.
Frasco, M.F., Truta, L.A.A.N.A., Sales, M.G.F., Moreira, F.T.C., 2017. Sensors 17 (3), 523.
Gabudean, A.M., Biro, D., Astilean, S., 2011. J. Mol. Struct. 993 (1), 420–424.
Gao, F., Feng, S., Chen, Z., Li-Chan, E.C.Y., Grant, E., Lu, X., 2014. J. Food Sci. 79 (12), N2542–N2549.
Hong, S., Li, X., 2013. J. Nanomater. 9. ID 790323.
Hu, Y., Lu, X., 2016. J. Food Sci. 81 (5), N1272–N1280.
Jayanthi, V.S.P.K., Sankara, A., Das, A.B., Saxena, U., 2017. Biosens. Bioelectron. 91, 15–23.
Ji, W., Zhang, M., Wang, T., Wang, X., Zheng, Z., Gong, J., 2017. Talanta 165, 18–26.
Joseph, M.M., Narayanan, N., Nair, J.B., Karunakaran, V., Ramya, A.N., Sujai, P.T., Saranya, G., Arya, J.S., Vijayan, V.M., Maiti, K.K., 2018. Biomaterials 181, 140–181.
Kumar, P.S., Pastoriza-Santos, I., Rodríguez-González, B., Abajo, F.J.G., Liz-Marzán, L. M., 2008. Nanotechnology 19 (1), 015606.
Li, H., Jiang, J., Wang, Z., Wang, X., Liu, X., Yan, Y., Li, C., 2017. J. Colloid Interface Sci. 501, 86–93.
Li, L., Liu, C., Cao, X., Tan, L., Lu, W., 2017. Bioanalysis 9 (20), 1561–1572.
Li, Q., Lu, Z., Tan, X., Xiao, X., Wang, P., Wu, L., Shao, K., Yin, W., Han, H., 2017. Biosens. Bioelectron. 97, 59–64.
Lin, Y., Xu, G., Wei, F., Zhang, A., Yang, J., Hu, Q., 2016. J. Pharm. Biomed. Anal. 121, 135–140.
Liu, P., Liu, R., Guan, G., Jiang, C., Wang, S., Zhang, Z., 2011. Analyst 136 (20), 4152–4158.
Lu, W., Wang, Y., Cao, X., Li, L., Dong, J., Qian, W., 2015. New J. Chem. 39 (7), 5420–5430.
Lv, Y., Qin, Y., Svec, F., Tan, T., 2016. Biosens. Bioelectron. 80, 433–441.
Negrín-Montecelo, Y., Comesaña-Hermo, M., Kong, X.T., Rodríguez-González, B., Wang, Z., Pérez-Lorenzo, M., Govorov, A.O., Correa-Duarte, M.A., 2018. ChemCatChem 10 (7), 1561–1565.
Pang, S., Yang, T., He, L., 2016. Trends Anal. Chem. 85, 73–82.
Scarabelli, L., Sánchez-Iglesias, A., Pérez-Juste, J., Liz-Marzán, L.M.A., 2015. J. Phys. Chem. Lett. 6 (21), 4270–4279.
Shahar, T., Sicron, T., Mandler, D., 2017. Nano Res. 10 (3), 1056–1063.
Shashni, B., Horiguchi, Y., Kurosu, K., Furusho, H., Nagasaki, Y., 2017. Biomaterials 134, 143–153.
Shi, L., Buhler, E., Boué, F., Carn, F., 2017. J. Colloid Interface Sci. 492, 191–198.
Sivanesan, A., Izake, E.L., Agoston, R., Ayoko, G.A., Sillence, M., 2015. J. Nanobiotechnol. 13 (1), 43.
Song, C., Min, L., Zhou, N., Yang, Y., Yang, B., Zhang, L., Su, S., Wang, L., 2014. RSC Adv. 4 (78), 41666–41669.
Song, C., Yang, Y., Yang, B., Min, L., Wang, L., 2016. J. Mat. Chem. B 4 (10), 1811–1817.
Song, G., Zhou, H., Gu, J., Liu, Q., Zhang, W., Su, H., Su, Y., Yao, Q., Zhang, D., 2017. J. Mat. Chem. B 5 (8), 1594–1600.
Sousa-Castillo, A., Ameneiro-Prieto, Ó., Comesaña-Hermo, M., Yu, R., Vila-Fungueiriño, J.M., Pérez-Lorenzo, M., Rivadulla, F., García de Abajo, F.J., Correa-Duarte, M.A., 2017. Nano Energy 37, 118–125.
Sousa-Castillo, A., Comesaña-Hermo, M., Rodríguez-González, B., Pérez-Lorenzo, M., Wang, Z., Kong, X.T., Govorov, A.O., Correa-Duarte, M.A., 2016. J. Phys. Chem. C 120 (21), 11690–11699.
Sun, C., Zhang, R., Gao, M., Zhang, X., 2015. Anal. Bioanal. Chem. 407 (29), 8883–8892.
Turkevich, J., Stevenson, P.C., Hillier, J., 1951. Discuss. Faraday Soc. 11 (0), 55–75, 1951.
Vasapollo, G., Sole, R.D., Mergola, L., Lazzoi, M.R., Scardino, A., Scorrano, S., Mele, G., 2011. Int. J. Mol. Sci. 12 (9), 5908.
Vidal, J.C., Garcia-Ruiz, E., Castillo, J.R., 2003. Microchim. Acta 143 (2), 93–111.
Vo-Dinh, T., 2018. J. Immunol. Sci. 2, 1–8, 2018.
Wallace, G.G., Smyth, M., Zhao, H., 1999. Trends Anal. Chem. 18 (4), 245–251, 1999.
Wang, F., Cao, S., Yan, R., Wang, Z., Wang, D., Yang, H., 2017. Sensors 17 (11), 2689.
Wang, M., Cao, X., Lu, W., Tao, L., Zhao, H., Wang, Y., Dong, J., Qian, W., 2016. J. Nanosci. Nanotechnol. 16 (7), 6711–6718.
Wang, Y., Yan, B., Chen, L., 2013. Chem. Rev. 113 (3), 1391–1428.
Wu, X., Xia, Y., Huang, Y., Li, J., Ruan, H., Chen, T., Luo, L., Shen, Z., Wu, A., 2016. ACS Appl. Mater. Interfaces 8 (31), 19928–19938.
Xue, J.Q., Li, D.W., Qu, L.L., Long, Y.T., 2013. Anal. Chim. Acta 777, 57–62.
Yang, K., Hu, Y., Dong, N., Zhu, G., Zhu, T., Jiang, N., 2017. Biosens. Bioelectron. 94, 286–291.
Ye, J., Chen, Y., Liu, Z., 2014. Angew. Chem. Int. Ed. 53 (39), 10386–10389.
Ye, J., Hutchison, J.A., Uji-i, H., Hofkens, J., Lagae, L., Maes, G., Borghs, G., Van Dorpe, P., 2012. Nanoscale 4 (5), 1606–1611.
Zhang, Y., Zhao, S., Zheng, J., He, L., 2017. Trends Anal. Chem. 90, 1–13.
Zoski, C.G., 2007. Handbook of Electrochemistry. Elsevier Science, p. 934.